

published in "Progress in Superconductivity Research" NOVA Science Publisher New-York (2007).

VAN HOVE SCENARIO FOR HIGH T_c SUPERCONDUCTORS

J. Bok and J. Bouvier*****

*Laboratoire Matériaux et Phénomènes Quantiques UMR 7162 - PARIS 7 -

**Solid State Physics Laboratory – ESPCI -

10, rue Vauquelin. 75231 PARIS Cedex 05, FRANCE

ABSTRACT

We give a general description of our approach which explains many physical properties in the superconducting and normal states of almost all 2D high T_c superconductors (HTSC). This 2D character leads to the existence of Van Hove singularities (VHs) or saddle points in the band structure of these compounds. The presence of VHs near the Fermi level in HTSC is now well established. We review some physical properties of these materials which can be explained by this scenario, in particular: the critical temperature T_c, the anomalous isotope effect, the superconducting gap and its anisotropy, and thermodynamic and transport properties (eg: Hall effect). The effects of doping and temperature are also studied, and they are directly dependent of the position of the Fermi level relative to the VHs position. We show that these compounds present a topological transition for a critical hole doping $p \approx 0.21$ hole per CuO₂ plane. Most of these compounds are disordered metals in the normal state, we think that the Coulomb repulsion is responsible for the loss of electronic states at the Fermi level, leading to a dip, or the so-called "pseudo-gap".

INTRODUCTION

Twenty years after the discovery of the high temperature superconductivity in cuprates compounds [1], the exact mechanism of superconductivity is still not yet understood. All these compounds are strongly anisotropic and almost two dimensional, due to their CuO₂ planes, where superconductivity mainly occurs. It is well known that in 2 dimensions, electrons in a periodic potential show a logarithmic density of states (DOS), named Van Hove singularity (VHs) (Van Hove (1953) [2]). The Van Hove scenario is based on the assumption that, in high critical temperature superconductors cuprates (HTSC), the Fermi

Level (FL) lies close to such a singularity (Labbé-Bok (1987)) [3]. This hypothesis has been confirmed by many experiments, in particular by Angular Resolved Photoemission Spectroscopy (ARPES) [4-9] in different compounds as:

$\text{La}_{2-x}\text{Sr}_x\text{CuO}_{4-\delta}$ (LSCO), $\text{Bi}_2\text{Sr}_2\text{CuO}_6$ (Bi 2201), $\text{Bi}_2\text{Sr}_2\text{CaCu}_2\text{O}_8$ (Bi 2212), $\text{YBa}_2\text{Cu}_3\text{O}_{7-\delta}$ (Y123), $\text{YBa}_2\text{Cu}_4\text{O}_8$ (Y124) and $\text{Nd}_{2-x}\text{Ce}_x\text{CuO}_{4+\delta}$ (NCCO). These experiments establish a general feature: in very high T_c superconductors cuprates ($T_c \sim 90$ K) Van Hove singularities are present close to the Fermi level. This is probably not purely accidental and we think that any theoretical model must take into account these experimental facts.

The origin of high T_c in the cuprates is still controversial and the role of these singularities in the mechanism of high T_c superconductivity is not yet established, but we want to stress that the model of 2D itinerant electrons in presence of VHS in the band structure has already explained a certain number of experimental facts.

In this review paper:

We recall what are the VHS physics in 1, 2, 3 dimensions.

We give a rapid description of the band structure of the CuO_2 planes.

We compute the critical temperature T_c [3,10,11], the anisotropic superconducting gap [10]. We show the importance of screening and Coulomb repulsion [10,12]. We explain the anomalous isotope effect [13], the very small values of the coherence length [14,15].

We compute the DOS in these compounds and apply this result to the calculations of various physical parameters: the conductance of tunnelling junctions, the specific heat [11], the magnetic susceptibility [16]. The variation of all these properties with hole doping (from underdoped UD to overdoped OD samples) and temperature are obtained and compared with the experiments. The agreement is very satisfactory. The variation with the doping is linked to the distance of the FL from the singularity level ($\xi_F - \xi_S$), so does the variation with the temperature due to the Fermi-Dirac distribution.

Transport properties in the normal state are described. We show that $\xi_F - \xi_S$ is critical for these properties, leading to Fermi liquid or marginal Fermi liquid [17].

We compute the Hall coefficient and its variation with doping and temperature [18]. We show that the experimental results may be explained by the topology of the Fermi surface (FS) which goes from hole-like to electron-like as the hole doping is increased. The critical doping, for which a topological transition is observed and calculated is $p = 0.21$ hole per CuO_2 plane.

A so-called “pseudo-gap” is observed in the normal state of cuprates. These compounds are disordered metals if we refer to their coefficient of diffusion, which is very low. The Coulomb interaction between electrons must be taken into account as shown by Altshuler and Aronov (1985) [19]. The main effect is to open a dip in the DOS at the FL. We show that this explains the observed features of the “pseudo-gap”, value, anisotropy and variation with doping [20].

In conclusion we show that VHS play an important role in HTSC, and that by taking them into account, we may explain most of their normal and superconducting properties.

VHS PHYSICS IN 1, 2, 3 DIMENSIONS

Van Hove singularities (2) are general features of periodic systems. They are topological properties of the electronic band structure (BS) and do not depend on the particular form of the BS. In one dimension (1D), they give a divergence of the DOS varying as $1 / \sqrt{\xi - \xi_s}$, where ξ_s is the energy of the singularity level. In two dimensions (2D), near VHs the variation of the DOS is logarithmic varying as:

$$\ln \left[\frac{D}{\xi - \xi_s} \right]$$

(Figure 1) where $D/2$ is the width of the singularity. In three dimensions (3D) the divergence is removed and we have a truncated 2D DOS.

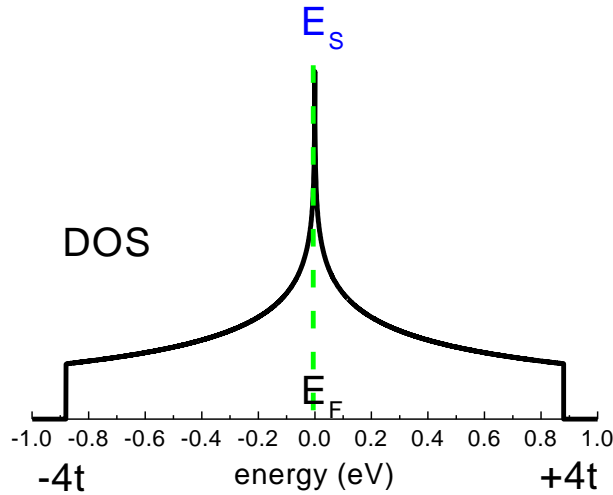


Figure 1: Density of States of a 2D system. ($E_F \equiv \xi_F$)

CALCULATION OF T_c

Labbé-Bok [3] have computed the band structure for the bidimensional CuO_2 planes of the cuprates, considered as a square lattice (quadratic phase). The simplest band structure we can take for a square lattice is :

$$\xi_{\mathbf{k}} = -2t [\cos k_x a + \cos k_y a] \quad (1)$$

where t is an interaction with nearest neighbours. This gives a square Fermi surface with saddle points, or VHs., at $[0, |\pi|]$ positions of the Brillouin zone (B.Z.), and a logarithmic D.O.S. with a singularity : $n(\xi) = n_1 \ln |D / (\xi - \xi_s)|$. The VHs. corresponds to half filling in this first calculation. We know that is not a good representation of the high T_c cuprates

because for half filling (one electron per copper site) they are antiferromagnetic insulators. We think that the Fermi level is at VHS. for a doping level corresponding to 21 % of holes in each CuO_2 plane or 0.395 filling of the first B.Z., this is confirmed by the observations of Ino *et al* [7]. This can be achieved by taking into account the repulsive interaction between second nearest neighbours (s.n.n.) and the effect of the rhomboedric distorsion. For the repulsive interaction with s.n.n. the band structure becomes:

$$\xi_{\mathbf{k}} = -2t \left[\cos k_x a + \cos k_y a \right] + 4\alpha t \cos k_x a \cos k_y a \quad (2)$$

where $\alpha t \equiv t'$ is an integral representing the interaction with s.n.n.. The singularity occurs for $\xi = -4\alpha t$, there is a shift towards lower energy. The Fermi surface at the VHS. is no longer a square but is rather diamond-shaped. More detailed calculations can be obtained in reference [14], taking also into account the rhomboedric distorsion.

The Labbé-Bok [3] formula was obtained using the following assumptions :

- 1- the Fermi level lies at the van Hove singularity
 - 2- the B.C.S. approach :
- The electron-phonon interaction is isotropic and so is the superconducting gap Δ .
 - The attractive interaction V_p between electrons is non zero only in an interval of energy $\pm \hbar\omega_0$ around the Fermi level where it is constant. When this attraction is mediated by emission and absorption of phonons, ω_0 is a typical phonon frequency.

In that case, the critical temperature is given by

$$k_B T_c = 1.13D \exp \left[- \left(\frac{1}{\lambda} + \ln^2 \left(\frac{\hbar\omega_0}{D} \right) - 1.3 \right)^{1/2} \right] \quad (3)$$

where $\lambda = (1/2) n_1 V_p$ is equivalent to the coupling constant.

A simplified version of formula (1), when $\hbar\omega_0$ is not too small compared to D , is :

$$k_B T_c = 1.13D \exp(-1/\sqrt{\lambda})$$

The two main effects enhancing T_c are

- 1- the prefactor in formula [3] which is an electronic energy much larger than a typical phonon energy $\hbar\omega_0$.

2- λ is replaced by $\sqrt{\lambda}$ in formula (3) in comparison with the BCS formula, so that in the weak coupling limit when $\lambda < 1$, the critical temperature is increased. In fact it gives too high values of T_c , we shall see later that this is due to the fact that we have neglected Coulomb repulsion between electrons. Taking this repulsion into account we shall obtain values for T_c which are very close to the observed one.

As it is however, this approach already explains many of the properties of the high T_c cuprates near optimum doping.

- The variation of T_c with doping

The highest T_c is obtained when the Fermi level is exactly at the VHs in this first calculation (formula (1)). For lower or higher doping the critical temperature decreases. That is what is observed experimentally [11].

- The isotope effect

Labbé and Bok [3] showed using formula (3) , that the isotope effect is strongly reduced for high T_c cuprates. Tsuei *et al* [21] have calculated the variation of the isotope effect with doping and shown that it explains the experimental observations.

- Marginal Fermi liquid behaviour

In a classical Fermi liquid, the lifetime broadening $1/\tau$ of an excited quasiparticle goes as ε^2 . The marginal Fermi liquid situation is the case where $1/\tau$ goes as ε . Theoretically marginal behaviour has been established in two situations (a) the half-filled nearest-neighbour coupled Hubbard model on a square lattice and (b) the Fermi level lies at a VHs (17,21). Experimental evidence of marginal Fermi liquid behaviour has been seen in angle resolved photoemission [22], infrared data [23] and temperature dependence of electrical resistivity [17]. Marginal Fermi liquid theory, in the frame work of VHs predicts a resistivity linear with temperature T. This was observed by Kubo et al [24]. They also observe that the dependence of resistivity goes from T for high T_c material to T² as the system is doped away from the maximum T_c, which is consistent with our picture; in lower T_c material the Fermi level is pushed away from the singularity.

INFLUENCE OF THE COULOMB REPULSION

It was also been shown that the singularity is in the middle of a wide band and that in these circumstances, the Coulomb repulsion μ is renormalized and μ is replaced by a smaller number μ^* [25] , the effective electron-phonon coupling is $\lambda_{\text{eff}} = \lambda - \mu^*$ and remains positive [15]. We think that this fact explains the very low T_c observed in Sr₂RuO₄, where a very narrow band has been determined by ARPES [26].

Cohen and Anderson [27] have shown that the electron-electron repulsion plays a central role in superconductivity. Assuming a constant repulsive potential $V_{\mathbf{k}\mathbf{k}'} = V_c$ from 0 to ξ_F they find that T_c is given by:

$$T_c \cong T_0 \exp \left[\frac{-1}{\lambda - \mu^*} \right] \quad (4)$$

$$\text{With } \mu = N_0 V_c \quad \text{and} \quad \mu^* = \frac{\mu}{1 + \mu \ln \xi_F / \omega_0}$$

Cohen and Anderson [27] assumed that for stability reasons μ is always greater than λ . Ginzburg [28] gave arguments that in some special circumstances μ can be smaller than λ . Nevertheless if we take $\mu \geq \lambda$, superconductivity only exists because μ^* is of the order of $\mu/3$ to $\mu/5$ for a Fermi energy ξ_F of the order of $100 \hbar \omega_0$. It is useless to reduce the width of the band W, because λ and μ vary simultaneously and μ^* becomes greater if ξ_F is reduced, thus giving a lower T_c. Superconductivity can even disappear in a very narrow band if $\lambda - \mu^*$ becomes negative.

We have shown [15] that high T_c can be achieved in a metal containing almost free electrons (Fermi liquid) in a broad band, with a peak in the D.O.S. near the middle of the band.

Taking a D.O.S., which is a constant n_0 between energies $[-W/2, -D]$ and $[+W/2, +D]$ (the zero of energy is at the Fermi level) and is $n(\xi) = n_1 \ln|D/\xi| + n_0$ between $-D$ and $+D$ we find for T_c , the following formula:

$$k_B T_c = \frac{D}{2} \exp \left[0.819 + \frac{n_0}{n_1} - \sqrt{F} \right] \quad (5)$$

where

$$F = \left(\frac{n_0}{n_1} + 0.819 \right)^2 + \left(\ln \frac{\hbar\omega_0}{D} \right)^2 - 2 - \frac{2}{n_1} \left(n_0 \ln \frac{2.28\hbar\omega_0}{D} - \frac{1}{V_p - V_c^*} \right)$$

$$V_c^* = \frac{V_c}{1 + V_c \left[\frac{n_1}{2} \left(\ln \frac{D}{\hbar\omega_0} \right)^2 + n_0 \ln \frac{W}{2\hbar\omega_0} \right]}$$

We can have a few limiting cases for this formula : $n_1 = 0$: no singularity. We find the Anderson-Morel formula. $V_c = 0$ and $n_0 = 0$: this gives the Labbé-Bok (L.B.) formula.

There are many effects enhancing T_c

$\lambda - \mu^*$ is reduced by the square root, down to $\sqrt{\lambda_1 - \mu_1^*}$ when n_1 is large enough.

As $\lambda - \mu^* < 1$ the critical temperature is strongly increased because this factor appears in an exponential. The prefactor before the exponential is D , the singularity width instead of $\hbar\omega_0$. We expect $D > \hbar\omega_0$. For instance D may be of the order of 0.5 eV and $\hbar\omega_0$ about a few 10 meV ($D/\hbar\omega_0$ of the order of 5 to 10).

We have made some numerical calculations using formula (5) to illustrate the effect of Coulomb repulsion. We used two values of D : $D = 0.9$ eV corresponding to $t = 0.25$ eV and a much more smaller value $D = 0.3$ eV. These calculations show that the Coulomb repulsion does not kill superconductivity in the framework of the L.B. model. The general rule for high T_c in this model is to have a peak in the density of states near the middle of a broad band to renormalize the effective repulsion μ . For a narrow band, W , or D , is small, T_c decreases very rapidly as seen in Figure 2 . A recent case has been observed in Sr_2RuO_4 with a narrow band and T_c is small [26].

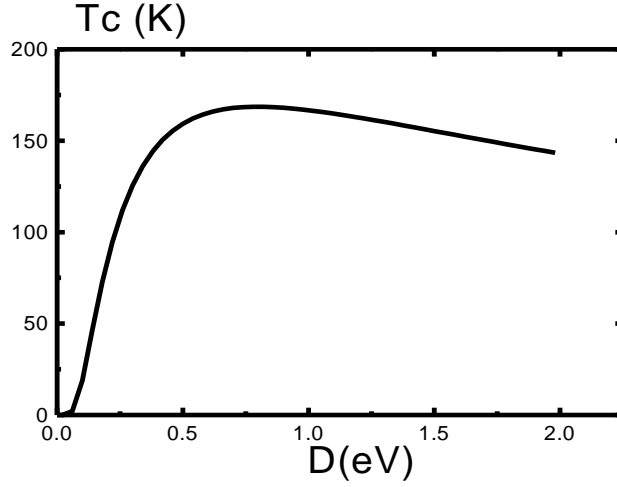


Figure 2: Effect of the width of the singularity D on T_c . n_0 and the total number of electrons per unit cell are maintained constant with this set of parameters.

Then $W = 2$ eV, $n_0 = 0.3$ eV/states/Cu, $n_1 = 0.2/D$.

In all these cases the calculations are made so that the total number of states of the band is one by Cu atom. Then $n_0 W + 2 n_1 D = 1$, and $\lambda = (n_0 + n_1) V_p$. In all these cases $\hbar\omega_0 = 0.05$ eV and $\lambda = 0.5$.

GAP ANISOTROPY

Bouvier and Bok [10] have shown that using a weakly screening electron-phonon interaction, and the band structure of the CuO_2 planes four saddle points: an anisotropic superconducting gap is found.

1. Model and basic equations

We use the rigid band model, the doping is represented by a shift $D_e = \xi_F - \xi_s$ of the Fermi level. This band structure is

$$\xi_{\mathbf{k}} = -2t \left[\cos k_x a + \cos k_y a \right] - D_e \quad (6)$$

The Fermi level is taken at $\xi_{\mathbf{k}} = 0$.

We use a weakly screened attractive electron-phonon interaction potential :

$$V_{\mathbf{k}\mathbf{k}'} = \frac{-|g_{\mathbf{q}}|^2}{q^2 + q_0^2} < 0$$

where $g(\mathbf{q})$ is the electron phonon interaction matrix element for $\vec{\mathbf{q}} = \vec{\mathbf{k}'} - \vec{\mathbf{k}}$ and q_0 is the inverse of the screening length.

We use reduced units: $X = k_x a$, $Y = k_y a$, $Q = qa$, $u = \frac{\xi}{2t}$, $\delta = \frac{D_e}{2t}$

We use the B.C.S. equation for an anisotropic gap :

$$\Delta_{\bar{k}} = \sum_{k'} \frac{V_{kk'} \Delta_{k'}}{\sqrt{\xi_{k'}^2 + \Delta_{k'}^2}} \quad (7)$$

We compute $\Delta_{\bar{k}}$ for two values of \bar{k} : Δ_A for $k_x a = \pi$, $k_y a = 0$ (8)

$$\Delta_B \text{ for } k_x a = k_y a = \frac{\pi}{2}$$

We solve equation (7) by iteration. We know from group theory considerations, that $V_{kk'}$ having a four-fold symmetry, the solution Δ_k has the same symmetry. We then may use the angle Φ between the 0 axis and the \bar{k} vector as a variable and expand $\Delta(\Phi)$ in Fourier series:

$$\Delta(\Phi) = \Delta_0 + \Delta_1 \cos(4\Phi + \varphi_1) + \Delta_2 \cos(8\Phi + \varphi_2) + \dots \quad (9)$$

We know that $\varphi_1 = 0$, because the maximum gap is in the directions of the saddle points. We use the first two terms. The first step in the iteration is obtained by replacing Δ_k by $\Delta_{av} = \Delta_0$ in the integral of equation (9). We thus obtain, for the two computed values : $\Delta_A = \Delta_{Max} = \Delta_0 + \Delta_1$ and $\Delta_B = \Delta_{min} = \Delta_0 - \Delta_1$, the following expression :

$$\Delta_{A,B}(T) = \lambda_{\text{eff}} \int_{u_{\min}}^{u_{\max}} \frac{\Delta_{av}}{\sqrt{u^2 + u_{av}^2}} I_{A,B}(u) \tanh\left(\frac{\sqrt{u^2 + u_{av}^2}}{k_B T / t}\right) du \quad (10)$$

$$\text{with } I_{A,B}(u) = \int_0^{x'_0} \frac{dx'}{\left[-\left[\delta - u \right] - \cos x' \right]^{1/2}} \frac{Q_{A,B}^2 + (q_0 a)^2}{Q_{A,B}^2 + (q_0 a)^2} \quad (11)$$

where $u_{\min} = -\frac{\hbar\omega_c}{2t}$, $u_{\max} = +\frac{\hbar\omega_c}{2t}$, $u_{av}(T) = \frac{\Delta_{av}(T)}{2t}$, $x'_0 = a \cos\left(\frac{\delta - u}{2}\right)$

ω_c is the cut off frequency. In the following part of this work we will keep the value of $\hbar\omega_c = 60$ meV for the Bi2212 compound, a characteristic experimental phonon energy. This choice respects our approximation for $V_{kk'}$.

- For the choice of t , the transfer integral comes from the photoemission experiments and is $t = 0.2$ eV as explained in Reference [10].

- $q_0 a$ is adjusted, it is the Thomas Fermi approximation for small q 's,

- λ_{eff} is adjusted so as to find the experimental value of Δ_{Max} and Δ_{min} and we find a reasonable value of about 0.5. λ_{eff} is the equivalent of $\lambda - \mu^*$ in the isotropic 3D, BCS model.

In fact the values of $q_0 a$ and λ_{eff} must depend of the hole doping level linked to D_e .

Here $q_0 a = 0.12$ and $\lambda_{\text{eff}} = 0.665$.

2. Results

In Figure 3, we present the result of the iterative calculation (formula 7-11).

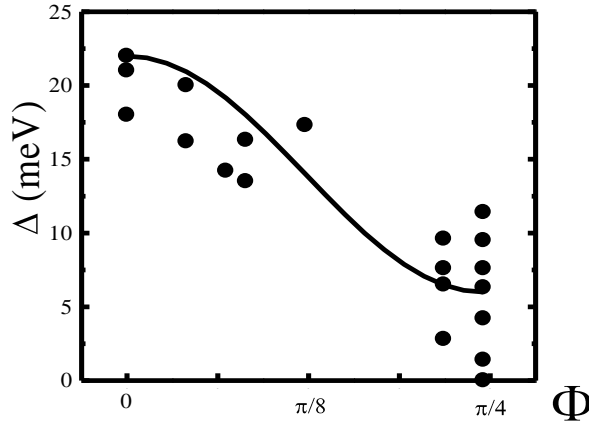


Figure 3: Anisotropic superconducting gap. Exact calculation for $\Phi = 0$ and $\pi/4$
This represents a s-wave anisotropic superconducting gap with no nodes in $\Phi = \pi/4$

In Figure 4, we present the variation of the various gaps Δ_{Max} , Δ_{min} and Δ_{av} with temperature at optimum doping, i.e. for a density of holes of the order of 0.20 per CuO_2 plane. We take in that case $D_e = 0$ and we find $T_c = 91$ K and an anisotropy ratio $\alpha = \Delta_{\text{Max}}/\Delta_{\text{min}} = 4.2$ and for the ratios of $2\Delta/k_B T_c$ the following values :

$$\frac{2\Delta_{\text{Max}}}{k_B T_c} = 6. , \quad \frac{2\Delta_{\text{av}}}{k_B T_c} = 3.7 , \quad \frac{2\Delta_{\text{min}}}{k_B T_c} = 1.4$$

This may explain the various values of $2\Delta/k_B T_c$ observed in experiments. Tunneling spectroscopy gives the maximum ratio and thermodynamic properties such as $\lambda(T)$ (penetration depth) gives the minimum gap.

In Figure 5 we present the same results, Δ_{Max} , Δ_{min} , Δ_{av} as a function of $D_e = \xi_F - \xi_s$ linked to the variation of doping.

In Figure 6 we plot the variation of the anisotropy ratio $\alpha = \Delta_{\text{Max}}/\Delta_{\text{min}}$ versus D_e . In Figure 7 the critical temperature T_c versus dx (variation of hole in the CuO_2 plane) from the optimal doping 0.20 hole per CuO_2 plane at $dx=0$, dx is linked in our calculation to the variation of D_e .

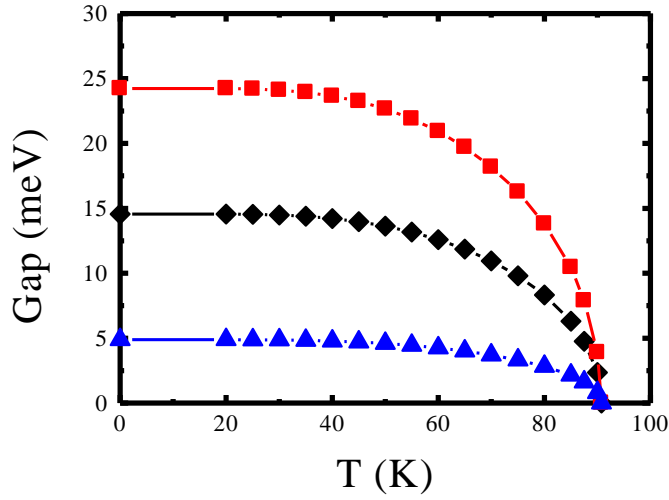


Figure 4: Variation of the various gaps Δ_{Max} , Δ_{min} and Δ_{av} versus temperature, at the optimum doping, i.e $D_c = \xi_F - \xi_s = 0$ in our model. With the following parameters, $t = 0.2$ eV, $\hbar\omega_c = 60$ meV, $q_0a = 0.12$, $\lambda_{\text{eff}} = 0.665$.

The critical temperature found is $T_c = 90.75$ K

red square symbol = Δ_{Max} , black diamond symbol = Δ_{av} , blue up triangle symbol = Δ_{min}

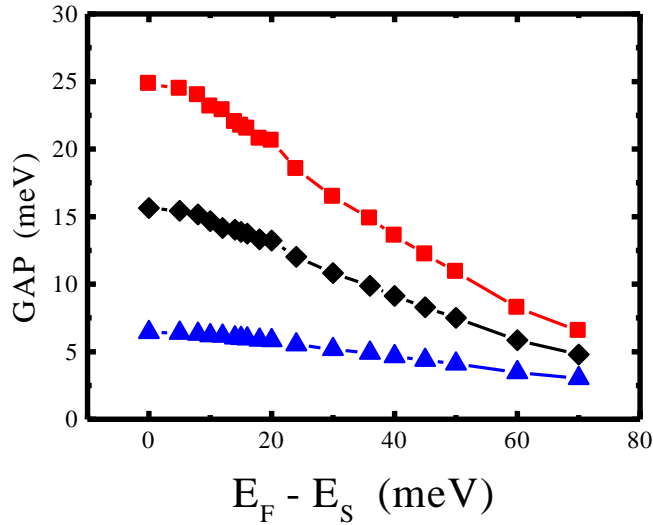


Figure 5: Variation of the various gaps Δ_{Max} , Δ_{min} , Δ_{av} versus $D_c = \xi_F - \xi_S \equiv E_F - E_S$, at $T = 0$ K
red square symbol = Δ_{Max} , black diamond symbol = Δ_{av} , blue up triangle symbol = Δ_{min}

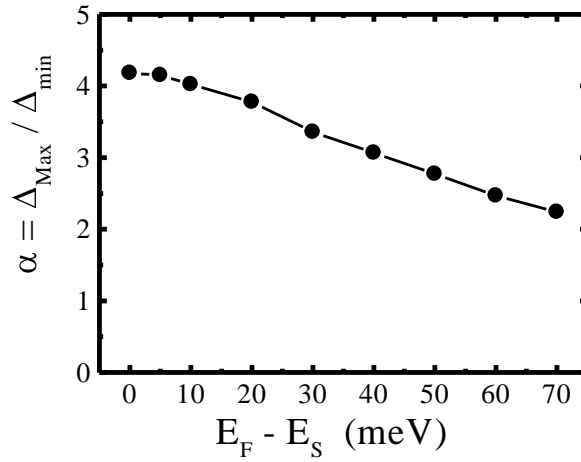


Figure 6: Variation of the anisotropy ratio $\alpha = \Delta_{\text{Max}}/\Delta_{\text{min}}$, versus $D_e = \xi_F - \xi_S \equiv E_F - E_S$.

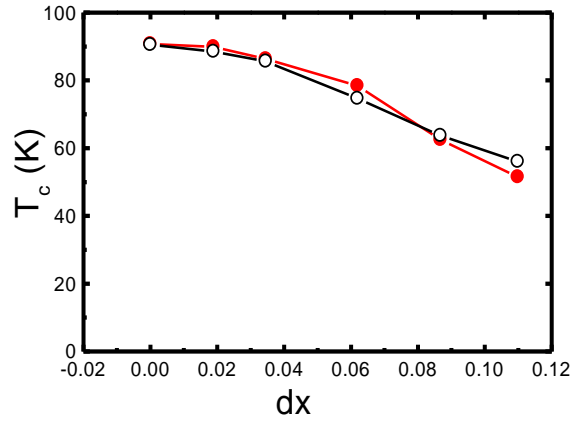


Figure 7: Comparison of the variation of T_c versus the variation of doping dx calculated in our model (red filled circles) and the experimental results of Koike et al ref [29] (black open circles).

We observe of course that T_c and the gaps decrease with D_e or dx . The agreement with experiment [29] is very good Figure 7. We obtain a new and interesting result which is the decrease of the anisotropy ratio α with doping. This is confirmed by results on photoemission [30,31] where a maximum gap ratio $2\Delta_{\text{Max}}/k_B T_c = 5$ to 7 is observed at optimum doping with $T_c = 83$ K and $2\Delta_{\text{Max}}/k_B T_c = 3$ for an overdoped sample with $T_c = 56$ K, with a small gap $\Delta_{\text{min}} = 0.2$ meV for the both T_c , for a Bi2212 compound.

DENSITY OF STATES AND TUNNELING SPECTROSCOPY

We have calculated the density of states of quasiparticle excitations in the superconducting state of high T_c [11,32] cuprates using the model of anisotropic gap that we have developed [10,32].

Here the D.O.S. is computed using the formula :

$$n(\varepsilon) = \frac{1}{2\pi^2} \frac{\partial A}{\partial \varepsilon} \quad (12)$$

where A is the area in k space between two curves of constant energy of the quasiparticle excitation ε_k given by : $\varepsilon_k^2 = \xi_k^2 + \Delta_k^2$ (13)

where ξ_k is the band structure (formula (6)). We use the same procedure and the same expression of Δ_k as before.

Figure 8 represents the variation of the D.O.S. as a function of ε for $T = 0$ K. This is similar to the experimental conductance (dI/dV versus the voltage V) of a N-I-S junction here we show the measurement made by Renner and Fisher [33] on a BSCCO sample. Δ_{Max} is located at the maximum peak and Δ_{min} at the first shoulder after the zero bias voltage, Figure 9. But for different values of $\xi_F - \xi_s$, we see a new maximum emerging, which is a signature of the van Hove singularity and a dip between this maximum and the peak at Δ_{Max} . This dip is seen experimentally in the STM tunneling experiments of Renner et al [33]. Figure 10 show the behaviour in fonction of the temperature, the value of the superconducting gap dependant in temperature are done by our calculations with formula (7-11).

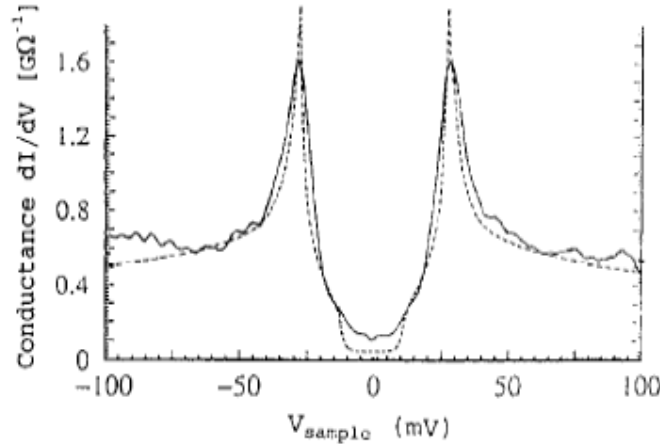


Figure 8: The best fit of the conductance measured by tunneling spectroscopy on BSCCO, N-I-S junction, by Renner and Fischer (Figure (10) of Reference [33]). solid line: fitted curve with $\Delta_{\text{Max}} = 27$ meV, $\Delta_{\text{min}} = 11$ meV, $t = 0.18$ eV, $\Gamma = 0.5$ meV at $T = 5$ K, dashed line : experimental curve.

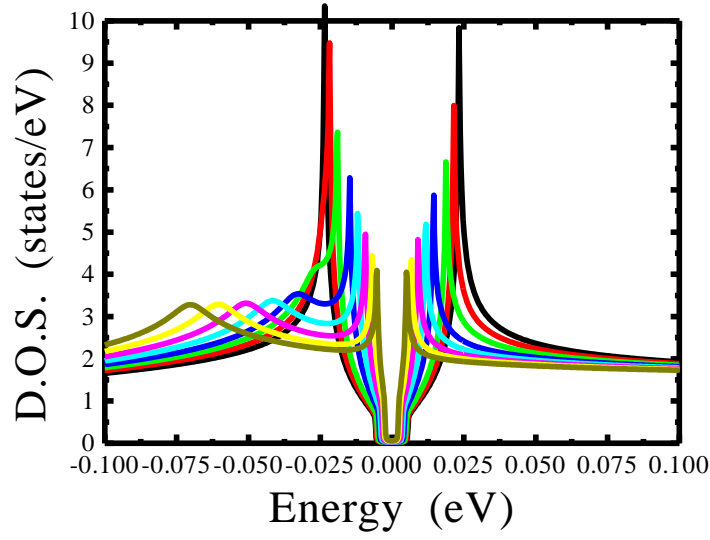


Figure 9: Variation of the D.O.S. versus the energy ϵ , for $T = 0$ K, that is similar at a NIS junction, for different values of the doping $D = \xi_F - \xi_{ss}$, i.e. 0, 10, 20, 30, 40, 60 and 70 meV with $\Gamma = 0.1$ meV and $\Gamma' = 5$ meV in the model of Reference [32].

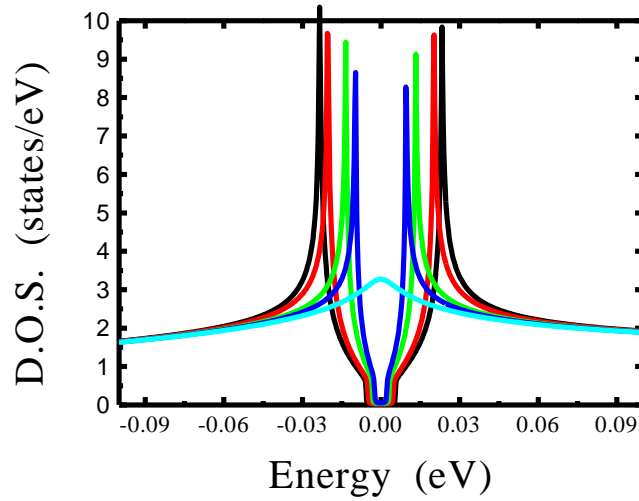


Figure 10: Variation of the in function of temperature $T = 0, 60, 80, 85, 91, T_c = 90.8$ K, for the case $\xi_F = \xi_s = 0$.

For the calculation of the conductance, we use the following formula

$$\frac{dI}{dV} = CN_0 \int_{-\infty}^{+\infty} N_S(\epsilon) \left[-\frac{\partial f_{FD}}{\partial V}(\epsilon - V) \right] d\epsilon \quad (14)$$

where f_{FD} is the usual Fermi-Dirac function; I and V are the current and voltage, C a constant proportional to $|T|^2$, the square of the barrier transmission, N_0 the D.O.S. of the normal metal that we assume constant, and $N_s(\epsilon)$ the previously calculated D.O.S. in the anisotropic superconductor. We introduce a damping parameter Γ in order to take into account the effect of a low 3D interaction and of the surface impurities.

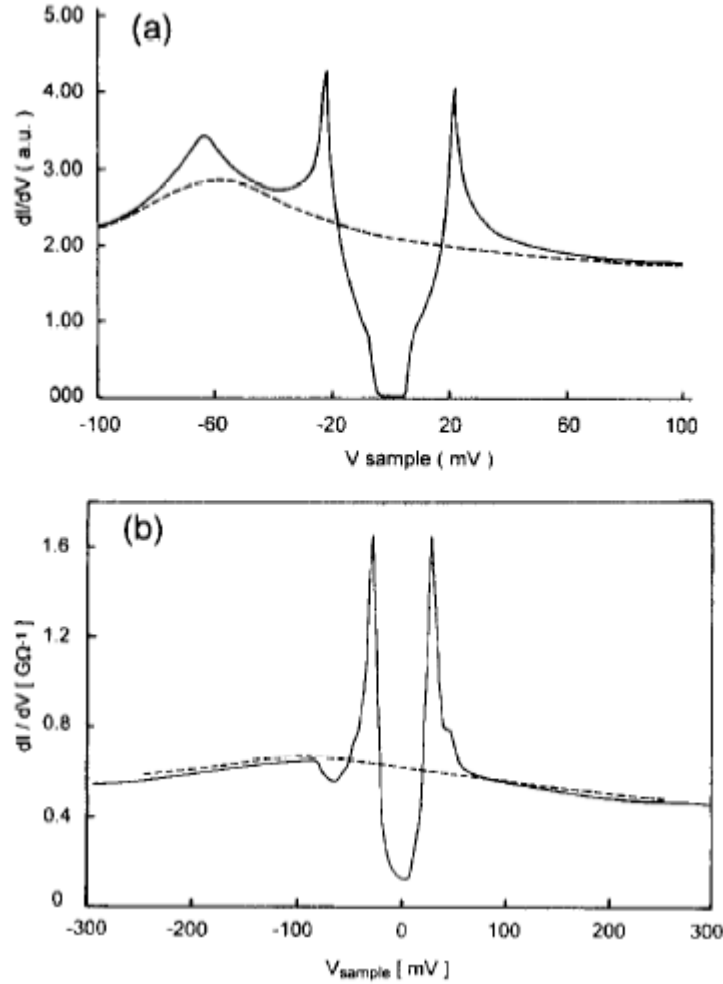


Figure 11: (a) Curves of the conductance calculated for a N-I-S junction. Solid line: in the superconducting state at $T = 5$ K with $\Delta_{Max} = 22$ meV, $\Delta_{min} = 6$ meV, $\Gamma = 0.1$ meV, $t = 0.2$ eV and $D_e = -60$ meV, $\Gamma' = 5$ meV. Dashed line : in the normal state at $T = 100$ K with $\Delta_{Max} = \Delta_{min} = 0$ meV, $\Gamma = 0.1$ meV, $t = 0.2$ eV and $D_e = -60$ meV, $\Gamma' = 5$ meV. (b) For comparison we show Figure (7) of Reference [33]. The maximum of the normal state conductance (or D.O.S.) at negative sample bias is well reproduced.

SPECIFIC HEAT

1. Theoretical calculation

The purpose of this chapter is to evaluate the influence of the VHs and the anisotropy of the gap on the specific heat calculated in the mean field B.C.S. approximation, i.e. we do not take into account the fluctuations near the critical temperature T_c . There are a great number of experiments measuring C_s . To compare our calculations to experiments, we must subtract the part due to fluctuations. These kind of adjustment have been made by various authors by using the fact that thermodynamic fluctuations are symmetric about T_c and can be easily evaluated above T_c [34,35]. Also we do not take into account the magnetic fluctuations in low temperature, nor the pair-breaking which may exist in overdoped sample. By the usual way, we obtain for C_s :

$$C_s(T) = \frac{2}{k_B T^2} \sum_k \frac{\exp(\epsilon_k / k_B T)}{\left(1 + \exp(\epsilon_k / k_B T)\right)^2} \epsilon_k^2 - \frac{1}{k_B T} \sum_k \frac{\exp(\epsilon_k / k_B T)}{\left(1 + \exp(\epsilon_k / k_B T)\right)^2} \frac{\partial \Delta_k^2(T)}{\partial T} \quad (15)$$

We use the values of ϵ_k and Δ_k ($\Delta_{\text{Max}}(T, D_e)$ and $\Delta_{\text{min}}(T, D_e)$) given by formula (7-11) to evaluate the two integrals of formula (15) numerically. Near T_c we have a very good agreement between the calculated values and the following analytical formula :

$$\Delta_{\text{Max,min}} = \Delta_{\text{Max,min}}(T=0) 1.7 \left(1 - (T/T_c)\right)^{3/2}$$

We see that the slopes $\partial \Delta^2 / \partial T$ do not depend on doping which simplifies the calculation of the second integral of formula (15). The results are presented in Figures 12 and 13 where we plot C_s versus T and $\Delta C/C|_{T_c}$ for various doping levels D_e .

We can make the following observations :

1- The jump in specific heat varies with doping $\Delta C/C|_{T_c}$ is 3.2 for $D_e = 0$ and 1.48 for $D_e = 60$ meV compared to 1.41, the B.C.S. value for a isotropic superconductor, with a constant D.O.S., N_0 in the normal state. The high value of $\Delta C/C|_{T_c}$ is essentially due to the VHs when it coincides with the Fermi level and the highest value of the gap Δ_k . With doping, the VHs moves away from ξ_F and $\Delta C/C|_{T_c}$ decreases toward its B.C.S. value.

2 - There is also a difference in the specific heat C_N in the normal state. For a usual metal with a constant DOS N_0 , $\gamma_N = C_N / T$ is constant and proportional to N_0 . Here we find $\gamma_N = a \ln(1/T) + b$ for $0 \leq D \leq 30$ meV where a and b are constant. For $D_e = 0$ this

behaviour has already been predicted by Bok and Labbé in 1987 [36]. The specific heat $C_N(T)$ explores a domain of width $k_B T$ around the Fermi level ξ_F . So for $D_e \ll k_B T_c$, the variation of γ_N above T_c is logarithmic. For $D_e > 30$ meV, at high temperature $T - T_c > D_e$, the B. L. law is observed, but for lower temperatures γ_N increases with T and passes through a maximum at T^* , following the law : $T^* \text{ (meV)} = 0.25 D_e \text{ (meV)}$ or $T^* \text{ (K)} = 2.9 D_e \text{ (meV)}$.

2. Comparison with experiments

Because of the difficulty to extract exactly C_s from the experimental data, we will compare only the general features to our calculation. We see that the doping has a strong influence on T_c and all the superconducting properties, so we assume that its role is to increase the density of holes in the CuO_2 planes. To compare our results on the effect of doping on C_s with experiments, we have chosen the family of the $\text{Tl}_2\text{Ba}_2\text{CuO}_{6+\delta}$, studied by Loram et al [37], Figure. 9 of Reference [37], because they are overdoped samples, with only one CuO_2 plane. The family $\text{YBa}_2\text{Cu}_3\text{O}_{6+x}$ is underdoped for $x < 0.92$ and for $x > 0.92$ the chains become metallic and play an important role. However, recent results by Loram et al, Figure 2a of the Reference [38] on Calcium doped YBCO, $\text{Y}_{0.8}\text{Ca}_{0.2}\text{Ba}_2\text{Cu}_3\text{O}_{7-\delta}$, which are overdoped two dimensionnal systems, show a very good agreement with our results. We notice the displacement and the decrease of the jump in specific heat C_s with doping. The jump $\Delta C/C|_{T_c} = \Delta\gamma/\gamma|_{T_c} = 1.67$ [37], and 1.60 [38] greater than the B.C.S. value 1.41 for a metal with a constant DOS. We find theoretically this increase in our model due to the logarithmic VHS. The symmetrical shape of the peak of C_s , at low doping level, is due to the critical fluctuations. A subtraction of these fluctuations [34,35] gives an asymmetrical shape. For high doping levels the classical B.C.S. shape is found.

For $D_e = 0$, we find that γ_N is not constant but given by the logarithmic law [36]: $\gamma_N = a \ln(1/T) + b$. When D_e increases, the law changes, γ_N passes through a maximum for a value of T , T^* . This behaviour is clearly seen in the YBCuO_{6+x} family [37]. We explain the high value $\Delta C/C|_{T_c} = 2.5$ for $x = 0.92$ in the YBCO family, and we find also the predicted variation of T^* .

Our model, neglecting magnetic fluctuations gives an Arrhenius law for C_s at low temperature with a characteristic energy which is Δ_{\min} . We see that such a law is observed in $\text{YBaCuO}_{6.92}$ and for $\text{Tl}_2\text{Ba}_2\text{CuO}_6$ at optimum doping.

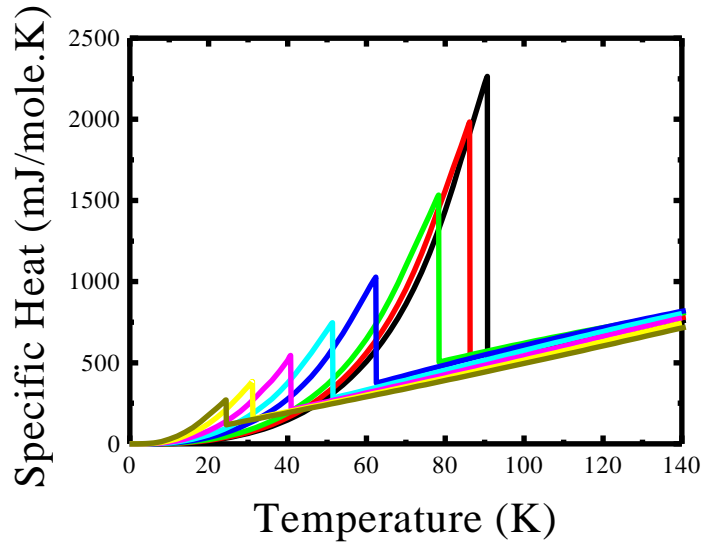


Figure 12: The calculated specific heat versus the temperature for the different value of $D_e = \xi_F - \xi_s = 0, 10, 20, 30, 40, 50, 60$ and 70 meV, linked to the variation of doping.

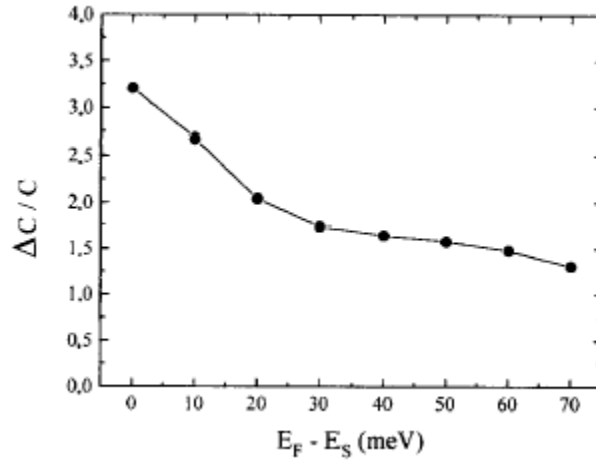


Figure 13: Variation of the jump in the specific heat, $\Delta C/C|_{T_c}$ versus D_e .

VAN HOVE SINGULARITY AND CHARACTERISTIC TEMPERATURE T°

Several experiments on photoemission, NMR and specific heat have been analyzed using a normal state pseudo-gap [39]. In fact, all what is needed to interpret these data is a density of state showing a peak above the Fermi energy. To obtain the desired D.O.S. several authors

[39] introduce a pseudogap in the normal state. This seems to us rather artificial, the above authors themselves write that the physical origin of this pseudogap is not understood.

We have shown that by using a band structure of the form formula (6), we may interpret the results obtained in the normal metallic state. We have computed the Pauli spin susceptibility using the following formula :

$$\chi_P = \frac{\mu_0 \mu_B}{B} \int_{-\infty}^{+\infty} \mathbf{n}(\xi) \left[f_{FD}(\xi + \mu_B \mathbf{B}) - f_{FD}(\xi - \mu_B \mathbf{B}) \right] d\xi \quad (16)$$

The results fit well the experiments. We find a characteristic temperature T° where the variation of χ_p versus T goes through a maximum. We may express $D_e = \xi_F - \xi_S$ as a variation of doping $\delta p = p - p_0$, p_0 being the doping for which $\xi_F - \xi_S$, $p_0 = 0.20$ hole/copper atom in the CuO_2 plane. Figure 14 the Pauli susceptibility in the normal state for the different value of the doping, from metallic system to the metal-insulator transition. Figure 15 represents the various experimental points taken from Figure 5 of Reference [39] where the authors plot $E_g/k_B T_{c\text{Max}}$ versus p . We see that what the authors call pseudogap is exactly our $D_e = \xi_F - \xi_S$, the distance from the Fermi level to the peak in the D.O.S..

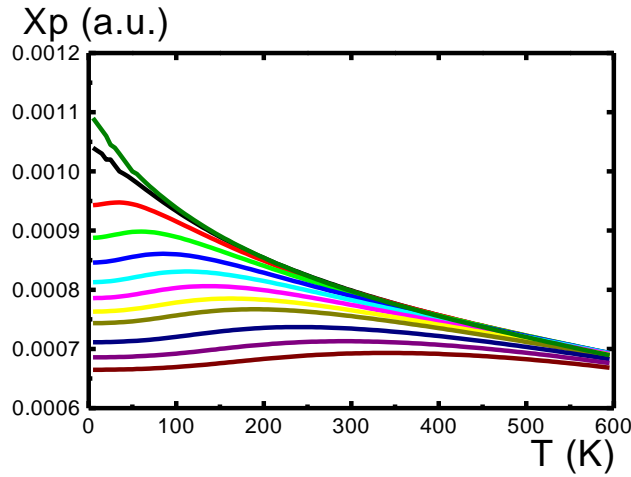


Figure 14: Pauli susceptibility in the normal state for the different value of the doping, decreasing from the top to the bottom. $\delta p = 0$, $p_0 = 0.20$ corresponding to the top curve, then δp varies from 0 to -0.15 , from metallic system to the metal-insulator transition.

δ

Figure 15: $D_e = \xi_F - \xi_S \equiv E_F - E_S$ divided by $k_B T_{cMAX}$ ($T_{cMAX} = 110$ K) versus the variation of the density of hole: solid line. The different symbols are the same as in the Figure 5 of the Reference [39], they represent the values of the so-called normal pseudogap divided by $k_B T_{cMAX}$ ($E_g / k_B T_{cMAX}$) obtained from NMR on different compounds. Our calculations are made with a transfer integral $t = 0.25$ eV, δp is taken as zero for $p = 0.20$.

o

δ

Figure 16: The temperature, T° , where the calculated χ_p (dashed line) and the specific heat (solid line) go through a maximum, versus δp . For comparison we show the results presented in Figure 27 of Reference [40], the symbols are the same. (solid squares : from thermoelectric power, circles : from specific heat, triangles: from NMR Knight shift data).

We have also computed the electronic specific heat C_s [11] in the normal state using the same DOS. We find that $\gamma = C_s/T$ goes through a maximum with temperature T , at a value T^* as found experimentally by Cooper and Loram [40]. In Figure 16 we compare our computed T^* with the experimental one (Reference [40]), the agreement is excellent. So we are able to interpret the NMR and specific heat data in the normal metallic state without invoking a pseudogap, but simply by taking into account the logarithmic singularity in the DOS.

We also explain the shift between the observed experimental optimum T_c , where $p = 0.16$ instead of 0.20, and the expected optimum T_c from our theory, i.e. where $D_e = 0$, by the fact that in first time in our gaps calculations we have not taking into account the variation of the 3D screening parameter q_0a in function of D_e . These calculations (see the following chapter) show the competition between the effect of the position of the V.H.s. and the value of q_0a for getting the optimum T_c , this competition depends on the compound. When the overdoping increases, i.e. the density of free carriers increases, then q_0a increases too, and in our model this leads to a decrease in T_c . It is why for $D_e = 0$, or $p = 0.20$, we have not the optimum T_c , and why the logarithmic law for χ_p is found in the overdoped range [11]. In the underdoped range in respect of the observed optimum T_c , (i.e. density of free carriers decrease), q_0a decreases too, but the Fermi level goes too far away from the singularity to obtain high T_c . Our results agree completely with the experimental observations.

EFFECT OF SCREENING ON THE GAP ANISOTROPY AND T_c

In the preceding part (“Gap Anisotropy” chapter) we have taken $q_0a = 0.12$ and the effective coupling constant $\lambda_{\text{eff}} = 0.665$ in order to fit the experimental values of the gap observed by ARPES and tunneling spectroscopy. We also have stressed the importance of q_0a in the value of the anisotropy ratio $\alpha = \Delta_{\text{Max}}/\Delta_{\text{min}}$. We shall now study in more details the influence of q_0a on α , T_c .

For α and T_c the calculations use equations 7-11 where q_0a is included in V_{kk} .

For α , we adjusted our values of λ_{eff} to obtain a constant critical temperature of 90.75 K and an average gap of $\Delta_{\text{av}} = 14.50 \pm 0.15$ meV. This approximation is valid in the limit of weak screening ($q_0a < 0.2$). The results are presented in Figure 17. We see that increasing q_0a , or in other word going towards more metallic system or 3D, that the anisotropy of the gap decreases. There are no direct experiments to measure α as a function of q_0a . The photoemission experiments measure the anisotropy as a function of doping, so q_0a and $\xi_F - \xi_S$ vary simultaneously. But there is a decrease in α when the doping is varying [30,31].

For T_c , we keep the parameter $D_e = 0 = \xi_F - \xi_S$ and we resolve the self-consistent equation (7) varying q_0a , and adjusting Δ_{Max} , Δ_{min} and Δ_{av} . The results are presented in Figure 18. The effect of increasing the screening strength is to decrease T_c . An increase of the screening can be due to the proximity of ξ_F to ξ_S where the DOS is high which leads to a strong screening, and in the other side the hide DOS increase T_c . It is why we have to take into account these two effects to explain the phase diagram (see the previous chapter).

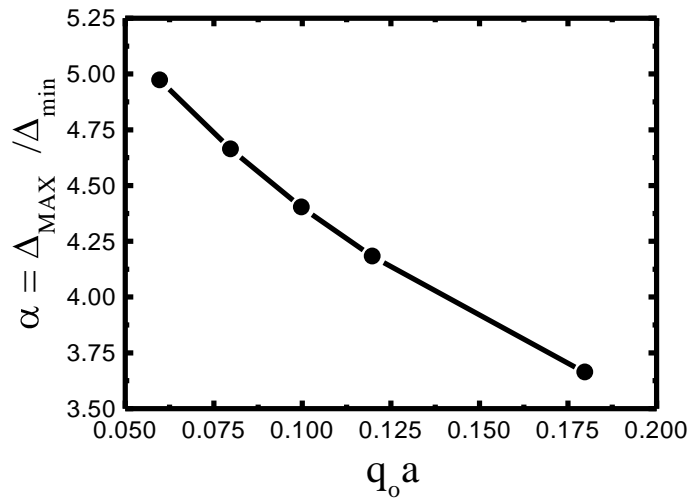


Figure 17: The anisotropy ratio $\alpha = \Delta_{MAX} / \Delta_{min}$ versus the screening parameter $q_0 a$.

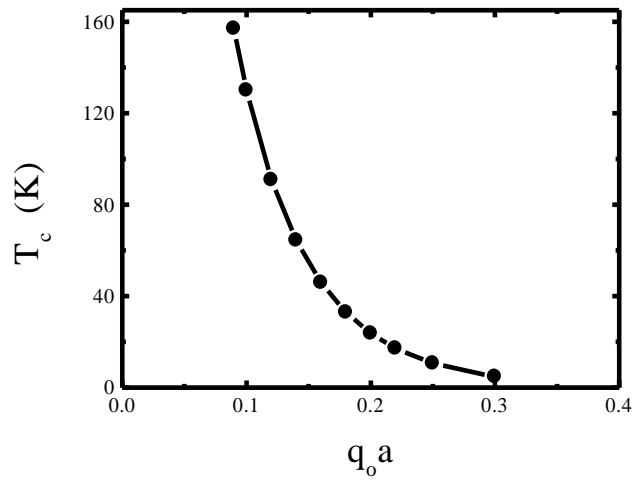


Figure 18: T_c versus the screening parameter $q_0 a$.

We have shown that the effect of increasing $q_0 a$ is to transform the system in a metallic or more isotropic one.

INFLUENCE OF DISORDER IN SUPERCONDUCTOR COMPOUNDS

We can consider underdoped or overdoped cuprates as disordered conductors because the diffusion coefficient D can be as low as $10^{-5} \text{ m}^2.\text{s}^{-1}$. Under these conditions Coulomb interaction between electrons must be taken into account. The main effect is to open a dip in the DOS near the Fermi level. We show that this model explains most of the observed features of the so-called “pseudogap” in the normal state including its value, anisotropy and variation with doping.

1. Introduction

Many experiments made in the normal state of high T_c superconductor have revealed a so-called pseudogap. This pseudogap was observed in transport, magnetic, specific heat measurements and in scanning tunneling and ARPES measurements [41]. The pseudogap observed in the normal state seems to be a partial gap. It is related to a crossover temperature, named T^* , below which its observation is possible. Many authors relate T^* with magnetic phenomena. We propose another explanation for the pseudogap related to T^* . It is mainly observed in underdoped samples, which are disordered and in which the mean free path and thus the diffusion coefficient is very low. Under these conditions, the diffusion length (L_D) becomes of the order of magnitude or smaller than the electron wavelength $1/k_F$. The materials are thus disordered conductors and the Coulomb repulsion becomes important (for a review see Altshuler and Aronov [19]).

2. Description of the model used

Altshuler and Aronov [19] have developed a theory to study the effect of the electron-electron interaction on the properties of disordered conductors. The conditions for its application $k_F L_D \ll 1$ is also satisfied for underdoped cuprates. The theory has also shown that the interaction effects are most clearly pronounced in low-dimensionality systems. We compute the one particle DOS taking into account the Coulomb interaction in the self-energy term. We show that particle repulsion produces a dip in the DOS at the Fermi energy. In the cuprates, where the Fermi surface is very anisotropic, we find that the pseudogap appears first and is more pronounced in the directions of the saddle points (1,0) and equivalent of the CuO_2 planes, where the Fermi velocity is smaller. This is clearly seen in the ARPES experiments.

We take an anisotropic dispersion relation for the one electron energy ξ_k in the CuO_2 planes (bidimensional):

$$\xi_k = -2t(\cos X + \cos Y) + 4t' \cos X \cos Y + D_e \quad (17)$$

where $D_e = \xi_F - \xi_S + 4 t'$

The self-energy is computed using the following formula:

$$\Sigma_m = \Sigma_m^{\text{ex}} + \Sigma_m^{\text{H}} \quad (18)$$

where Σ_m^{ex} is the exchange part and Σ_m^{H} the Hartree part of the self-energy.

The exchange energy is given by:

$$\Sigma_{\mathbf{m},\xi}^{\text{ex}} = \frac{1}{2\pi v_\xi} \int_{-\infty}^{\infty} d\omega \int_{\pi}^{\pi} \frac{d^3 \mathbf{q}}{\omega^2 + q^2} U(\vec{q}) \quad (19)$$

with $\vec{q} = \vec{k} - \vec{k}'$, D the diffusion coefficient. $U(\vec{q})$ is the Fourier transform of the long range Coulomb interaction and the term in Dq^2 the Fourier transform of the electron-electron correlation function. For $U(\vec{q})$ we take a screened Coulomb potential (the screening is tridimensional):

$$U(\vec{q}) = C / (q^2 + q_0^2) \quad (20)$$

where q_0^{-1} is the screening length. We then compute the DOS within a small angle $d\theta$, in the two directions (1,0) and (1,1), using a selfconsistent procedure.

3. Variation of the coefficient of diffusion D with doping and k space direction.

In a simple Fermi liquid, the diffusion coefficient is given by $D = (1/3)v_F l$, v_F is the Fermi velocity and l is the mean free path. For a given sample, with doping and disordered fixed, l is constant and v_F varies with direction, it is much smaller near the saddle point A ($0, \pm\pi$) than at point B ($\pm\pi/2, \pm\pi/2$). In underdoped samples there are disorder in the oxygen vacancies and crystalline defects. We assume that l is strongly reduced as the doping decreases until we reach a region where the crystalline order is restored in the insulating antiferromagnetic state. $\xi_F - \xi_S$ varies slightly and v_F at point A is reduced, v_F at point B remains almost unchanged, so the anisotropy remains.

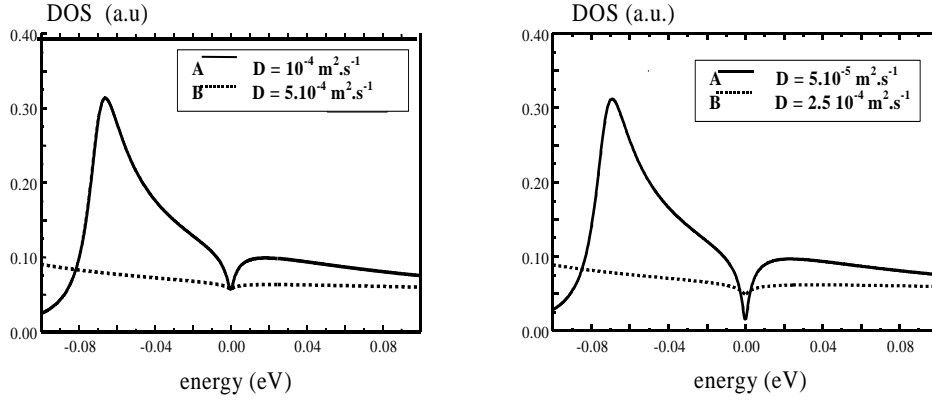


Figure 19: Calculated DOS with Coulomb interaction with different sets of values of D
 A : in the (1,0) direction, and equivalent directions - B : in the (1,1) direction

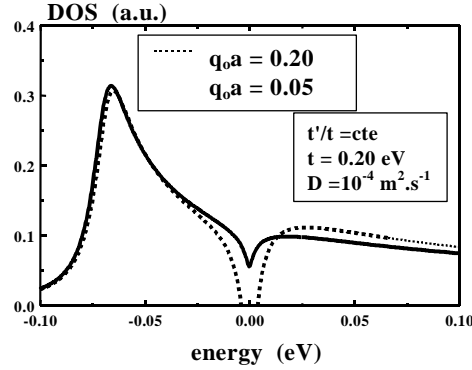


Figure 20: Effect of the screening on the DOS calculated with the Coulomb interaction term.

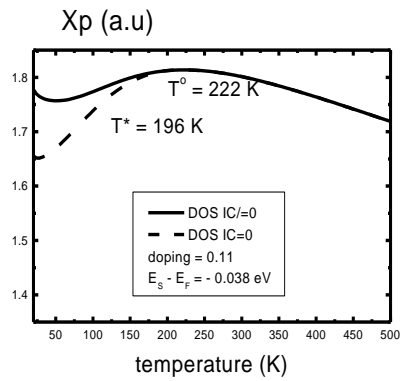
4. Effect of the the coefficient of diffusion, the screening and the bandwidth.

Our results are presented in Figure 19. We can see that our model explains why the pseudogap opens in the (1,0) direction and not in the (1,1) direction as seen in ARPES [41]. We have studied the effect of screening by varying $q_0 a$, in the A direction, the result is shown on Figure 20. The decrease of $q_0 a$ increases the number of states in the wings and deepens the dip. The effect of varying the transfer integrals, t and t' , i.e. the bandwidth, is less important.

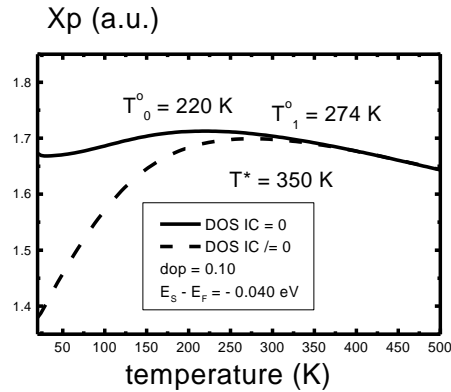
5. Pauli susceptibility and disorder

We are able to calculate the total DOS including the exchange term in the self-energy, the dip created at FL by the disorder effect can be more or less deep or broad, depending for a

given bandwidth of the coefficient of diffusion or the screening strength values. We study some cases and calculate the corresponding Pauli susceptibility, as already made but without disorder effect (see the previous chapter “VHs and T° ” and Reference [42], where the maxima in the $X_p(T)$ curves were related to the high DOS at ξ_S . In Figure 21 we present our theoretical results for two different pseudogaps. In Figure 21b it is deeper and broader, at T^* , where these pseudogaps open, $X_p(T)$ (dashed line) begins to be lower than $X_p(T)$ (full line) without pseudogap. In Figure 21a this opening occurs after the temperature T° , where the high DOS at E_S begins to be filled, but in Figure 21b this opening occurs before this event. The consequence of these mixing effects give an effective T°_1 in our initial theory [42] and $T^* > T^\circ$. This is a theoretical result to be discussed as all experimental results seem to give $T^\circ > T^*$. Such bigger pseudogap probably occurs for lower doping, leading to $T^* < T^\circ$.



(a)



(b)

Figure 21: Calculated Pauli Susceptibilities

Full line = without disorder effect - Dashed line = with disorder effect. Figure 21a: for 0.11 hole doping. Figure 21b: for 0.10 hole, lower doping, with a deeper and broader dip, leading to a smaller $X_p(T)$, to a more pronounced decrease, and to $T^* > T^\circ$.

6. Discussion

Experiments reported by I. Vobornik *et al* [43] show the possibility of having disorder-induced pseudogaps comparable to those existing in underdoped Bi2212 samples. The pseudogap can also be observed in overdoped samples [43]. As we can see in our figures, the dip is less pronounced if either the screening or the diffusion coefficient is higher. These higher values exist in the overdoped regime, leading to a lower value of T^* . Then it seems to be below T_c , so it cannot be observed in the normal state [44]. Therefore in varying the physical parameters in our model (screening, doping (i.e.: $\xi_F - \xi_S$), diffusion coefficient, bandwidth), we have a good explanation for the evolution of the pseudogap in the phase diagram. The pseudogap decreases from underdoped to overdoped region in agreement with these parameters. The pseudogap was observed in a non-superconducting region in scanning tunneling spectroscopy measurements made by T. Cren *et al* [45]. This shows that the pseudogap is not inevitably related to superconductivity, but is an intrinsic property of the material. The existence of the "Coulomb dip" in the HTSC and the Si doped metals [20,46], where we know it is due to disorder, confirms that disorder can be at the origin of the pseudogap.

HALL EFFECT IN THE NORMAL STATE OF HTSC

1. INTRODUCTION

Many measurements of the Hall coefficient R_H in various high T_c cuprates have been published [47-51]. The main results are the following :

- (i) at low temperature T , $R_H \approx 1/p_{h0}e$, where p_{h0} is the hole doping, when T increases R_H decreases, and for highly overdoped samples becomes even negative [47].
- (ii) these authors are also able to define a temperature T_0 , where R_H changes its temperature behaviour, and they found that $R_H(T)/R_H(T_0)$ versus T/T_0 is a universal curve for a large doping domain (from $p_{h0} = 0.10$ to $p_{h0} = 0.27$).

We can explain these results by using the band structure for carriers in the CuO_2 planes. In particular, the existence of hole-like and electron-like constant energy curves, which give contributions of opposite sign to R_H . The transport properties explore a range of energy $k_B T$ around the Fermi level, when T is increased more and more carriers are on the electron like orbits, resulting in a decrease of R_H .

2. CALCULATION OF THE HALL COEFFICIENT

The constant energy surfaces of carriers in the CuO_2 planes are well describe by formula 17. It is very clearly seen [7] that the Fermi level crosses the saddle points (or VHs), at ξ_S , for a hole doping of $p_{h0} \approx 0.22$. For energies $E > \xi_S$ the orbits are hole-like, and for $E < \xi_S$ they are electron-like.

To compute the Hall coefficient we use the formula obtained by solving the Boltzmann equation. In the limit of low magnetic fields B , perpendicular to the CuO_2 plane, $\mu B \ll 1$, where μ is an average mobility of the carriers, R_H is given by:

$$R_H = \frac{\sigma_{xy}}{\sigma_{xx}^2} \frac{1}{B} \quad (21)$$

where σ_{xy} and σ_{xx} are the components of the conductivity tensor. We follow the approach given by N. P. Ong [52]:

$$\sigma_{xy} = \int_{E_{\min}}^{E_{\max}} \left(-\frac{\partial f_0}{\partial E} \right) \sigma_{xy}(E) dE \quad (22)$$

where f_0 is the Fermi Dirac distribution function, E_{\min} and E_{\max} are the bottom and the top of the band, and $\sigma_{xy}(E)$ is σ_{xy} computed on a constant energy surface.

For metals, where $k_B T \ll \xi_F$, σ_{xy} is usually chosen as $\sigma_{xy} = \sigma_{xy}(\xi_F)$, computed on the Fermi surface only, this is done by N. P. Ong [52]. In our case, $k_B T$ is not small compared to $\xi_F - \xi_S$, so when T increases the electron-like orbits as well as the hole-like orbits are populated. The electron-like orbits give a negative contribution to R_H , so that R_H decreases with temperature. This is our original approach to the problem. To compute R_H , we use the following method: We compute first $\sigma_{xy}(E)$ using the Ong approach. The idea is to draw the \vec{l} curve swept by the vector $\vec{l} = \vec{v}_k \tau_k$ as \vec{k} moves around the constant energy curve (C.E.C.). Then σ_{xy} reduces to:

$$\sigma_{xy} = \frac{2e^3}{\hbar^2} A_l B \quad (23)$$

where A_l is the area enclosed by C.E.C., in the (l_x, l_y) plane. There may be secondary loops in the \vec{l} curve. When the C.E.C. is non-convex, the \vec{l} curve presents several parts where the circulation are opposite (see Reference [52] Figure 2). Then the effective density of carriers that must be taken in computing σ_{xy} is $n_e' = \Gamma n_e$ for the electron-like orbits, with $\Gamma < 1$, and $p_h' = p_h$ for the hole-like orbits, because for the hole-like orbits we can see that the C.E.C. have no non-convex parts. Finally we obtain for the Hall coefficient:

$$R_H = \frac{V}{e} \frac{p_h - b^2 n_e'}{p_h + b(p_{h0} - p_h)} \quad (24)$$

where b is the ratio of the average mobilities of the carriers on the electron and hole like orbits. That is the mean value of $\langle \tau / m \rangle$, where τ is the relaxation time and m the effective

mass. V is the volume of the unit cell. We adjust the Fermi level so that the total number of carriers p_{h0} remains constant. To compute Γ , we must know the scattering mechanisms and evaluate Γ . Γ was computed by Ong [52] assuming a constant \bar{l} , but this is not valid in our case because \bar{l} is very small near the saddle points (hot spot), both v_k and mainly the relaxation time τ_k are small at this point. So we estimated a much smaller value of Γ , around $\Gamma = 0.2$ for E near ξ_S and going to $\Gamma = 1$ when E approaches E_{\min} . We choose a function $\Gamma(E)$, varying from $\Gamma(\xi_S)$ to 1 for $\Gamma(E_{\min})$.

$$\Gamma(E) = 1 - \alpha \frac{(E - E_{\min})^n}{\xi_S - E_{\min}}$$

$$\alpha = \frac{1 - \Gamma(\xi_S)}{\xi_S - E_{\min}}, \quad \text{with } n = 1$$

n_e , p_h are given by the following formulae:

$$n_e = \int_{E_{\min}}^{E_S} A_e(E) \Gamma(E) \left(-\frac{\partial f_0}{\partial E} \right) dE \quad (25)$$

$$p_h = \int_{E_S}^{E_{\max}} A_e(E) \Gamma(E) \left(-\frac{\partial f_0}{\partial E} \right) dE \quad (26)$$

$$p_h = \int_{E_S}^{E_{\max}} A_h(e) \Gamma(E) \left(-\frac{\partial f_0}{\partial E} \right) dE \quad (27)$$

A_e is the area enclosed by the electron-like surfaces for $E < \xi_S$, A_h is the area enclosed by the hole-like surfaces for $E > \xi_S$. E_{\max} is determined in order to only take into account the holes added to the lower half-band. So we obtain for $T = 0$ K the density of free hole per CuO_2 plane, the Hall number $n_H = 1/(R_H e) = p_{h0}/V$. The scattering mechanism being probably the same for the electron and the hole orbits, which are very similar along the (1,1,0) direction, then we assume $b = 1$.

3. RESULTS

The results of our calculations and their comparison with the experimental results are given in Figures 22, 23, 24, 25. When the authors of the experiments give only the concentration x of doping atoms, and the critical temperature T_c we have to evaluate the actual hole doping p_{h0} using the universal phase diagram of T_c versus doping for high T_c superconductors [53].

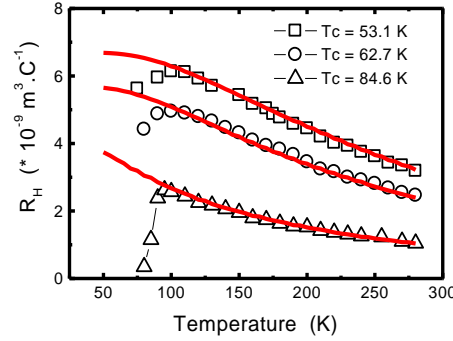


Figure 22:

symbols: experimental $R_H(T)$ given by Matthey et al (Reference [50]) in $\text{GdBa}_2\text{Cu}_3\text{O}_{7-\delta}$

full lines: theoretical fits

theoretical hole doping level $p_{h0} = 0.10$ for the experimental $T_c = 53.1$ K

theoretical hole doping level $p_{h0} = 0.12$ for the experimental $T_c = 62.7$ K

theoretical hole doping level $p_{h0} = 0.16$ for the experimental $T_c = 84.6$ K

The calculations are made with : $t = 0.18$ eV , $t' = 0.04328$ eV , $2t'/t = 0.48$, $\Gamma(\zeta_S) = 0.2$

For the theoretical results of Figures 22, 23, 24 we use the following parameters : $t = 0.18$ eV , $t' = 0.04328$ eV , $2t'/t = 0.48$, $\Gamma(\zeta_S) = 0.2$. These values of t and t' means that the shape of the Fermi surfaces changes when we cross the critical doping $p_{h0} \approx 0.22$. This is also seen in the photoemission curves reported by Ino et al [7].

In Figure 23 , we can see the representation of the universal law $R_H(T)/R_H(T_0)$ versus T/T_0 , where T_0 is defined experimentally by the fact that R_H becomes almost constant above this temperature [47-50]. In our model this temperature is given by $2k_B T_0 = \xi_F - \xi_S$, this shows that this universal behaviour is due to the 2D band structure, in which the shift $\xi_F - \xi_S$ is connected to the hole doping. This is very natural in our approach, because the factor $(\xi_F - \xi_S)/k_B T$ enters the Fermi-Dirac distribution.

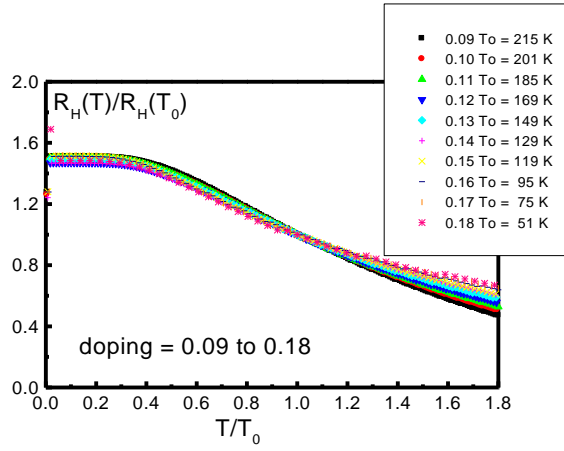
We see that the agreement of our fits with the experiments are excellent. There is a small discrepancy between the values of our theoretical R_H and the experimental values. We think that this is due to the inhomogeneities in the material and to the way to carry out the R_H measurements. This can may be explained by the evaluation of the experimental volume V . We use in our calculation the unit cell volumes:

$$V_{\text{LSCO}} \cong 189 \cdot 10^{-30} \text{ m}^3 \text{ for LSCO and } V_{\text{YBCO}} \cong 174 \cdot 10^{-30} \text{ m}^3 \text{ for YBCO.}$$

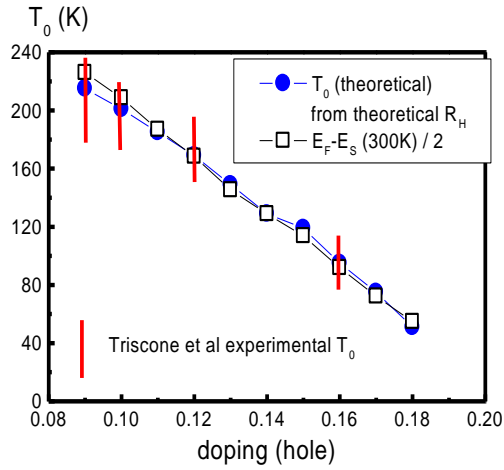
The experimental value of R_H is determined by the geometrical aspect of the sample (the thickness in particular). This value is evaluated assuming that the current flow is homogeneous throughout the sample, this is not always true. We find a discrepancy between 1.5 and 2 in the case of YBCO [48] and GdBCO [50], a larger discrepancy is found in the case of LSCO [47]. In this later case, the authors find different R_H results for the same doping, with various compounds (single crystals and thin films).

Anyway, adjusting our values for R_H , at low temperature, we can fit many experimental results, for the three different compounds. We also use a rigid band model, where the

bandwidth does not change with the doping. This is not exactly the case as shown in the photoemission experiments [51], but the effect is small and does not change our conclusions.



(a)



(b)

Figure 23:

a) : universal law $R_H(T)/R_H(T_0)$ versus T/T_0 for various hole doping levels, from 0.09 to 0.18.

b) : calculated T_0 , $2k_B T_0 = \xi_F - \xi_S$, compared with the experimental T_0 given by Matthey et al (Reference [50]).

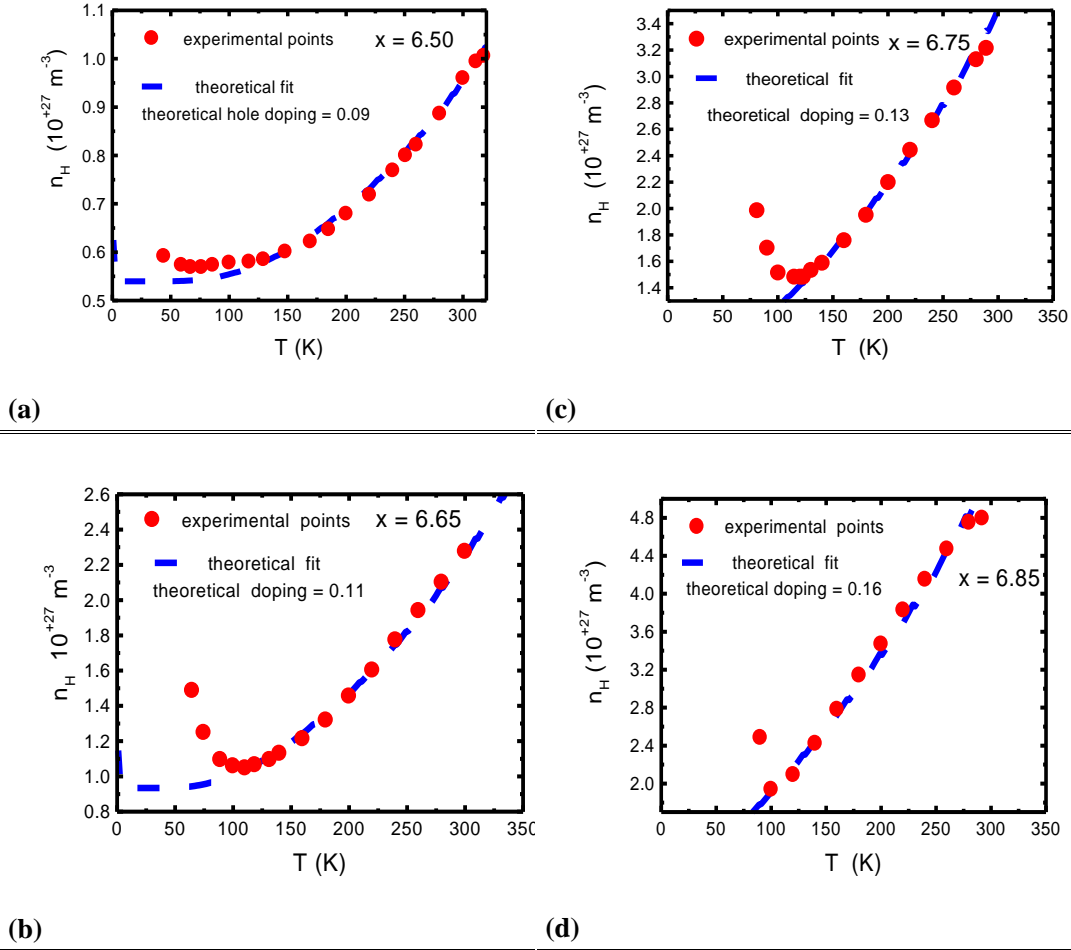


Figure 24:

Filled circles: experimental $n_H(T) = V/(R_H e)$ given by Wuyts et al (Reference [48]) in $YBa_2Cu_3O_x$.

Dashed lines: theoretical fits

- a) $x=6.50$, theoretical hole level = 0.09
- b) $x=6.65$, theoretical hole level = 0.11
- c) $x=6.75$, theoretical hole level = 0.13
- d) $x=6.85$, theoretical hole level = 0.16

The calculations are made with: $t = 0.18$ eV, $t' = 0.04328$ eV, $2t'/t = 0.48$, $\Gamma(\xi_s) = 0.2$ then we obtain the same universal law as in Figure 23a, expressed in $n_H(T)/n_H(T_0)$.

From overdoped to lightly underdoped samples the upturns, at low temperature, in the experimental curves are due to the occurrence of the superconductivity transition.

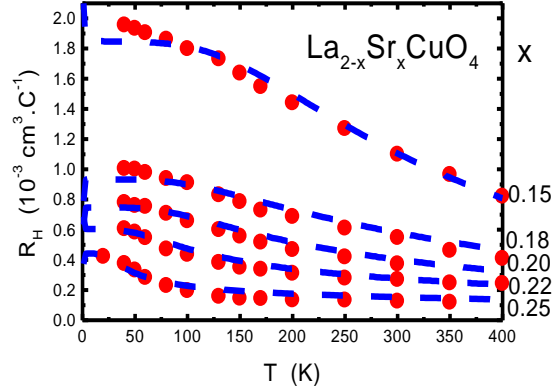


Figure 25: Filled circles: experimental $R_H(T)$ given by Hwang et al (Reference [47]), in polycrystalline $\text{La}_{2-x}\text{Sr}_x\text{CuO}_4$, for $x = 0.15, 0.18, 0.20, 0.22, 0.25$. Dashed lines: theoretical fits, the theoretical hole levels as the same as the experimental.

The calculations are made with : $t = 0.23$ eV, $t' = 0.06$ eV, $2t'/t = 0.52$, $\Gamma(\xi_S) = 0.1$

4. THEORETICAL RESULTS AND DISCUSSION

We use a theoretical band structure closed to the observed experimental one, but not in the fine details. We take a rigid band structure not varying with the doping, but we know that this variation occurs. Here we make our study with the ratio of transfer integrals of transfer closed to $2t'/t = 0.48$ in order to obtain this special doping $p_{h_0} \approx 0.22$ when $\xi_F = \xi_S$ as in our previous studies, leading to convincing results (see previous chapters and Reference [12]).

In Figures 22-25 , we give the best fits with the parameters that we need for this. The value of Γ maybe is too big because with our choice of t and t' the curvatures of the C.E.C. are not so pronounced as in reality.

But the aim of this chapter is to demonstrate that the temperature dependence of the Hall coefficient is due to the effect of the distribution of the hole carriers in the electron-like energy levels and in the hole-like energy levels with increasing temperature. The results of our model do not change appreciably if we change slightly our set of parameters.

Γ itself could change with the doping when the band structure varies. Near the optimum hole doped and overdoped systems Γ could decrease due to bigger curvatures of the C.E.C. In Figure 26 , we show the effect of the decreasing of Γ for a slightly overdoped system. This account for the behaviour of $R_H(T)$ in the optimum and slightly overdoped samples, where $R_H(T)$ is very flat and its value is very low closed to zero, and even can goes under zero at low or high temperature [47-49,51]. Theoretically this is due to the proximity of ξ_F and ξ_S .

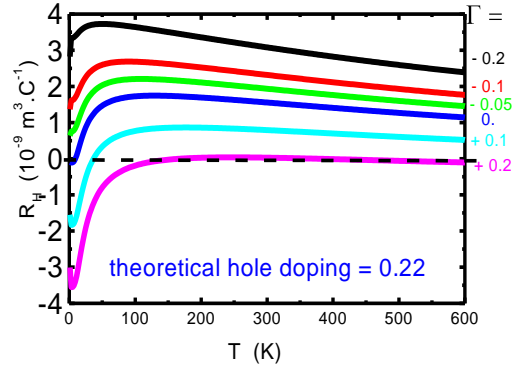


Figure 26: Theoretical curves of $R_H(T)$ showing the effect of Γ with, from the top to the bottom, the values: -0.2 , -0.1 , -0.05 , 0 , $+0.1$, $+0.2$. The calculations are made with: $t = 0.23$ eV, $t' = 0.0553$ eV, $2t'/t = 0.48$, $V_{YBCO} \cong 174 \cdot 10^{-30} \text{ m}^3$, for a theoretical hole doping = 0.22. As the curvatures of the orbits increase, Γ goes from positive to negative value. This leads to very low (even negative) values to higher positive values at low T, for $R_H(T)$ in the optimum and overdoped samples.

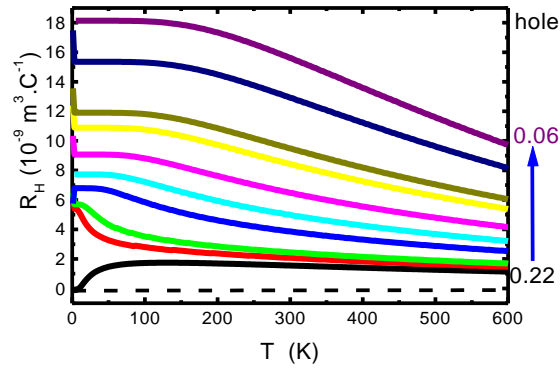


Figure 27: Theoretical curves of $R_H(T)$ with the same fit parameters of Figure 26 and with $\Gamma(\xi_S) = 0$. From the bottom to the top the hole dopings are the following : 0.22, 0.20, 0.19, 0.16, 0.14, 0.12, 0.10, 0.09, 0.07, 0.06.

In Figure 27, we show the theoretical $R_H(T)$ curves for a set of doping, using the same fit parameters as in Figure 26, letting $\Gamma(\xi_S) = 0$. We can see that the general behaviour of $R_H(T)$ is kept.

For very underdoped samples, near the metal-insulator transition our approach is no longer valid. We propose an explanation for the downturns observed in $R_H(T)$ [50,52] based on the localization of the carriers above an energy E_{loc} (see Figure 28).

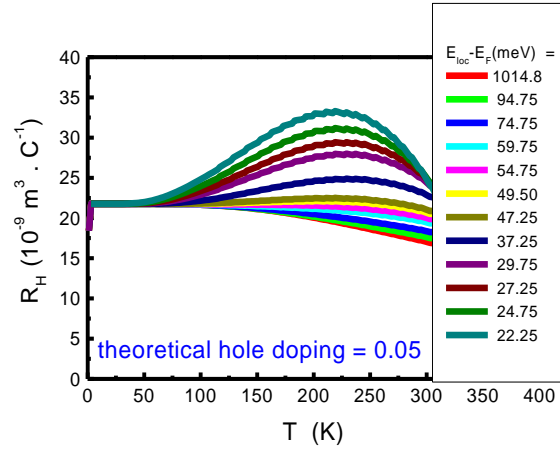


Figure 28: A localization level (E_{loc}) is introduced in the model to take into account the proximity of the metal-insulator transition in very underdoped sample.

The calculations are made for a hole doping of 0.05, with: $t = 0.18$ eV, $t' = 0.04328$ eV, $2t'/t = 0.48$, $\Gamma(\xi_s) = 0$, $V_{YBCO} \cong 174 \cdot 10^{-30} \text{ m}^3$.

From the bottom to the top of the Figure 28 $E_{loc} - \xi_F$ varies from +1015 meV, that means no localization, to +22 meV, effective localization. We see that a strong maxima appears when the localization increases. This is due to the loss of localized particles, which do not contribute to transport.

In conclusion we find that the electronic structure of CuO_2 planes, with hole-like and electron-like orbits can explain the values of R_H for the high T_c cuprates in the normal state and its temperature behaviour [54], this conclusion is reinforced by the fact that we obtain a representation of the experimental universal law $R_H(T)/R_H(T_0)$ versus T/T_0 .

CONCLUSION

In conclusion, we have proven that the Van Hove scenario explains many physical properties of the HTSC cuprates both in the normal and superconducting states. The existence of saddle points (VHs) close to the Fermi level is now well established by many experiments. This fact must be taken into account in any physical description of the properties of high T_c superconductors.

REFERENCES

- [1] J. G. Bednorz and K. A. Müller, *Z. A. Phys.* **B 64**, 189 (1986).
- [2] L. Van Hove, *Phys. Rev.* **89**, 1189 (1953).

- [3] J. Labbé, J. Bok, *Europhys. Lett.* **3**, 1225 (1987).
- [4] H. Ding, J. C. Campuzano, K. Gofron, C. Gu, R. Liu, B. W. Veal and G. Jennings. *Phys. Rev. B* **50**, 1333 (1994).
- [5] Z. X. Shen, W.E. Spicer, D.M. King, D.S. Dessau, B.O. Wells, *Science* **267**, 343 (1995).
- [6] Jian Ma, C. Quitmann, R.J. Kelley, P. Almería, H. Berger, G. Margaritondoni, M. Onellion. *Phys. Rev. B* **51**, 3832 (1995).
- [7] A. Ino, C. Kim, M. Nakamura, Y. Yoshida, T. Mizokawa, A. Fujimori, Z. X. Shen, T. Takeshita, H. Eisaki, and S. Uchida, *Phys. Rev. B* **65**, 094504 (2002).
- [8] T. Yoshida, X. J. Zhou, T. Sasagawa, W. L. Yang, P. V. Bogdanov, A. Lanzara, Z. Hussain, T. Mizokawa, A. Fujimori, H. Eisaki, Z.-X. Shen, T. Kakeshita, and S. Uchida, *Phys. Rev. Lett.* **91**, 027001 (2003)
- [9] M. Abrecht, D. Ariosa, D. Cloetta, S. Mitrovic, M. Onellion, X. X. Xi, G. Margaritondo, and D. Pavuna, *Phys. Rev. Lett.* **91**, 057002 (2003)
- [10] J. Bouvier and J. Bok, *Physica C* **249**, 117 (1995).
- [11] J. Bouvier and J. Bok, *Physica C* **288**, 217 (1997).
- [12] J. Bouvier, J. Bok. "Superconductivity in cuprates, the van Hove scenario: a review." In "The Gap Symmetry and Fluctuations in HTSC." Edited by Bok et al., Plenum Press, New York, 37 (1998).
- [13] J. Labbé and J. Bok, *Europhys. Lett.* **3**, 1225 (1987).
- [14] J. Bok and L. Force. *Physica C* **185**, 1449 (1991).
- [15] L. Force and J. Bok. *Solid Stat. Comm.* **85**, 975 (1993).
- [16] J. Bouvier and J. Bok, *J. of Superc.* **6**, 673 (1997).
- [17] P. C. Pattnaik C. L. Kane D. M. Newns and C. C. Tsuei. *Phys. Rev. B* **45**, 5714 (1992).
- [18] J. Bok, J. Bouvier, *Physica C* **403**, 263 (2004).

- [19] B.L. ALTSHULER and A.G. ARONOV, (Electron-Electron Interaction In Disordered Conductors, in : Electron-Electron Interaction In Disordered Systems, eds. A.L. Efros and M. Pollak. Elsevier Science Publishers B.V. (1985).
- [20] J. Bouvier, J. Bok, H. Kim, G. Trotter, M. Osofsky, *Physica C* **364**, 471 (2001).
- [21] C.C. Tsuei, D.M. Newns, C.C. Chi et P.C. Pattnaik, *Phys. Rev. Lett.* **65**, 2724 (1990).
- [22] C.G. Olson, R. Liu, D. W. Lynch R. S. List, A. J. Arko B. W. Veal, Y. C. Chang, P. Z. Jiang, and A. P. Paulikas, *Phys. Rev. B* **42**, 381 (1990).
- [23] Z. Schlesinger et al, *Phys. Rev. Lett.* **67**, 2741 (1991).
- [24] Y. Kubo, Y. Shimakawa, T. Manako, and H. Igarashi, *Phys. Rev. B* **43**, 7875 (1991).
- [25] P. W. Anderson and P. Morel, *Phys. Rev.* **125**, 4 (1962).
- [26] T. Yokoya, A. Chainini, T. Takashahi, H. Katayama-Yoshida, M. Kasai and Y. Tokura, *Physica C* **263**, 505 (1996).
- [27] M.L. Cohen and P.W. Anderson in *Superconductivity in d and f band Metals*, edited by D.H. Douglass (A.I.P. New York) (1972) .
- [28] V. Ginzburg, *Comtemporary Physics* **33**, 15 (1992).
- [29] Y. Koike, Yoshihiro Iwabuchi, Syoichi Hosoya, Norio Kobayashi and Tetsuo Fukase, *Physica C* **159**, 105 (1989).
- [30] M. Onellion, R.J. Kelley, D.M. Poirier, C.G. Olson and C. Kendziora, preprint "Superconducting energy gap versus transition temperature in $\text{Bi}_2\text{Sr}_2\text{CaCu}_2\text{O}_{8+x}$ ", R.J. Kelley, Jian Mia, C. Quitmann *Phys. Rev. B* **50**, 590 (1994).
- [31] R.J. Kelley, C. Quitmann, M. Onellion, H. Berger, P. Almeras and G. Margaritondo, *Science* **271** (1996) 1255.
- [32] J. Bok and J. Bouvier, *Physica C* **274**, 1 (1997).
- [33] Ch. Renner and O. Fisher, *Phys. Rev. B* **51**, 9208 (1995).
- [34] O. Riou, M. Charalambous, P. Gandit, J. Chaussy, P. Lejay and W.N. Hardy "Disymmetry of critical exponents in YBCO" published in *LT 21 proceedings*.

- [35] C. Marcenat, R. Calemczuk and A. Carrington, "Specific heat of cuprate superconductors near T_c " published in "Coherence in high temperature superconductors" edited by G. Deutscher and A. Revcolevski World Scientific Publishing Company (1996).
- [36] J. Bok and J. Labbé, *C.R. Acad. Sci Paris* **305**, 555 (1987).
- [37] J. W. Loram, K.A. Mirza, J.M. Wade, J.R. Cooper and W.Y. Liang, *Physica C* **235**, 134 (1994).
- [38] J.W. Loram, K.A. Mirza, J.R. Cooper, J.L. Tallon. published in the *proceedings of M²S-HTSC-V*, Feb 28-Mar 4, 1997, Beijing, China. *Physica C: Superconductivity, Volumes 282-287, Part 3, August 1997, Pages 1405-1406*
- [39] G.V.M. Williams, J.L Tallon, E.M. Haines, R. Michalak, and R. Dupree, *Phys. Rev Lett.* **78**, 721 (1997).
- [40] J.R. Cooper and J. W. Loram, *J. Phys. I France* **6**, 2237 (1996).
- [41] T. Timusk and B. Statt, *Rep. Prog. Phys.* **62**, 61 (1999).
- [42] J. Bouvier and J. Bok, *J. of Supercond.* **10**, 673 (1997).
- [43] I. Vobornik, H. Berger, D. Pavuna, M. Onellion, G. Margaritondo, F. Rullier-Albenque, L. Forró, and M. Grioni, *Phys. Rev. Lett.* **82**, 3128 (1999).
- [44] O. Fisher *et al* - P. Müller *et al* - D. Rubio *et al*, *J. of Superconductivity* **13** (2000).
- [45] T. Cren, D. Roditchev, W. Sacks, and J. Klein, *Phys. Rev. Lett.* **84** (2000) 147.
- [46] M. S. Osofsky, R. J. Soulen, Jr., J. H. Claassen, B. Nadgorny, J. S. Horwitz, G. Trotter and H. Kim, *Physica C* **364-365** (2001) 427.
- [47] H. Y. Hwang, B. Batlogg, H. Takagi, H. L. Kao, J. Kwo, R. J. Cava, J. J. Krajewski and W. F. Peck, *Phys. Rev. Lett* **16**, 2636 (1994).
- [48] B. Wuyts, V. V. Moshchalkov and Y. Bruynseraede, *Phys. Rev. B* **53**, 9418 (1996).
- [49] Z. Konstantinovic, Z. Z. Li and H. Raffy, *Physica C* **341-348**, 859 (2000).
- [50] D. Matthey, S. Gariglio, B. Giovannini and J.-M. Triscone, *Phys. Rev. B* **64**, 024513 (2001).

- [51] F. F. Balakirev, J. B. Betts, A. Migliori, S. Ono, Y. Ando, G. S. Boebinger, *Nature* **424**, 912 (2003).
- [52] N. P. Ong, *Phys. Rev. B* **43** (1991) 193.
- [53] J. Bobroff, H. Alloul, S. Ouazi, P. Mendels, A. Mahajan, N. Blanchard, G. Collin, V. Guillen, and J.-F. Marucco, *Phys. Rev. Lett* **89**, 157002 (2002).
- [54] J. Bok, J. Bouvier. *Physica C : Superconductivity* **403**, 263 (2004).